DOI 10.7343/as-2026-966

ACQUE SOTTERRANEE
Italian Journal of Groundwater

2026-AS56-966: 25 - 38

journal homepage: https://www.acquesotterranee.net/

Isotope and geochemical tracing for acid mine drainage impacts in coal mines areas of Pakistan

Analisi isotopica e geochimica degli impatti del drenaggio acido di miniera nelle aree minerarie del carbone del Pakistan

Abdul Ghaffar[a]

a - Isotope Application Division, Pakistan Institute of Nuclear Science and Technology (PINSTECH), Islamabad, Pakistan.

ARTICLE INFO

Ricevuto/*Received*: 31 January 2025
Accettato/*Accepted*: 11 March 2026
Pubblicato online/*Published online*: 30 March 2026

Handling Editor:
Andrea Citrini

Editor in Chief:
Rudy Rossetto

Citation:
Ghaffar, A. (2026). Isotope and geochemical tracing for acid mine drainage impacts in coal mines areas of Pakistan .
Acque Sotterranee - *Italian Journal of Groundwater*, 15(1), 25 - 38
https://doi.org/10.7343/as-2026-966

Correspondence to:
Abdul Ghaffar
ghaffargreat@pinstech.org.pk

Keywords:
active coal mining, stable isotopes, hydro-geochemistry, sulfate isotopes, sources of sulfates in groundwater, AMD impacts, Oxidation and dissolution processes.

Parole chiave:
estrazione carbonifera attiva, isotopi stabili, idrogeochimica, isotopi del solfato, sorgenti di solfati nelle acque sotterranee, impatti del drenaggio acido di miniera, processi di ossidazione e dissoluzione.

Abstract

Groundwater in coal mining regions is highly vulnerable to contamination from Acid Mine Drainage (AMD), posing significant environmental and public health risks. This study applied combined hydrogeochemical and stable/isotopic analyses to assess AMD impacts and recharge mechanisms in the active Pail-Padhrar coal mining area, Chakwal, Pakistan. Water samples were collected from mine sumps, surface bodies, and boreholes (purged prior to sampling), with field measurements of pH, electrical conductivity, and dissolved oxygen. Cations, anions, and trace metals were analyzed using AAS, ICP-OES, and UV-visible spectrophotometry, while $\delta^{18}O$, $\delta^{2}H$, $\delta^{34}S$, and $\delta^{18}O$ of sulfate were measured to trace recharge and geochemical processes. AMD-impacted waters were characterized by SO_4^{2-}–Cl^-–Na^+–Ca^{2+} hydrochemical types, high TDS, low pH, and signatures of sulfide oxidation, evaporation, and silicate weathering. Non-AMD-impacted waters exhibited SO_4^{2-}–Na^+–Ca^{2+} to Na^+–Ca^{2+}–HCO_3^- types, dominated by rock weathering, mineral dissolution, and ion exchange. Isotopic data confirmed precipitation as the primary recharge source, with d-excess values distinguishing rainwater mixing, evaporation, and AMD influence. Sulfate isotopes revealed pyrite oxidation and gypsum dissolution as major sulfate sources, supported by iron oxyhydroxide presence. These findings highlight the spatial heterogeneity of groundwater processes and provide a comprehensive framework for understanding AMD impacts on aquifer chemistry, essential for sustainable groundwater management in coal mining regions.
Key words: Active coal Mining; Stable isotopes; Hydro-Geochemistry; Sulfate isotopes; Sources of sulfates in groundwater, AMD impacts; Oxidation and dissolution processes.

Riassunto

Le acque sotterranee nelle regioni interessate da miniere di carbone sono altamente vulnerabili alla contaminazione da drenaggio acido di miniera (Acid Mine Drainage, AMD), con conseguenti rischi significativi per l'ambiente e la salute pubblica. Questo studio ha combinato analisi idrogeochimiche e isotopiche valutando gli impatti dell'AMD e i meccanismi di ricarica nell'area mineraria attiva di Pail-Padhrar, Chakwal, in Pakistan. I campioni d'acqua sono stati raccolti da pozzetti di miniera, corpi idrici superficiali e da fori di sondaggio (spurgati prima del campionamento), con misurazioni in campo di pH, conducibilità elettrica e ossigeno disciolto. Cationi, anioni e metalli in traccia sono stati analizzati mediante AAS, ICP-OES e spettrofotometria UV-visibile, mentre $\delta^{18}O$, $\delta^{2}H$, $\delta^{34}S$, e $\delta^{18}O$ dei solfati sono stati misurati per tracciare la ricarica e i processi geochimici.
Le acque influenzate dall'AMD risultano caratterizzate da facies idrochimica SO_4^{2-}–Cl^-–Na^+–Ca^{2+}, elevati valori di TDS, basso pH e firme riconducibili a ossidazione di solfuri, evaporazione e alterazione dei silicati. Le acque non influenzate dall'AMD mostravano invece facies SO_4^{2-}–Na^+–Ca^{2+} to Na^+–Ca^{2+}–HCO_3^- , dominati da alterazione delle rocce, dissoluzione minerale e scambio ionico. I dati isotopici hanno confermato la precipitazione come principale fonte di ricarica, con valori di d-excess che permettono di distinguere il mescolamento con acqua meteorica, l'evaporazione e l'influenza dell'AMD. Gli isotopi del solfato hanno rivelato che l'ossidazione della pirite e la dissoluzione del gesso sono le principali fonti di solfato, come confermato anche dalla presenza di idrossidi di ferro. Questi risultati evidenziano l'eterogeneità spaziale dei processi che interessano le acque sotterranee e forniscono un quadro interpretativo completo per comprendere gli impatti dell'AMD sulla chimica degli acquiferi, essenziale per una gestione sostenibile delle risorse idriche sotterranee in associazione alle miniere di carbone.

Introduction

Groundwater resources in coal mining areas are widely recognized as being highly vulnerable to contamination, which can have significant consequences for the natural environment (Bian et al., 2010). Water generated during mining operations may react with metallic sulfide minerals such as pyrite, arsenopyrite, and marcasite present in coal-bearing strata, leading to the formation of Acid Mine Drainage (AMD) (Sahoo and Khaoash, 2020; Connor et al., 2023). Acid mine drainage results from the exposure and subsequent oxidation of sulfide minerals during and after mining activities, and it can contaminate both surface water and groundwater systems (Nordstrom, 2011). AMD significantly increases the solubility and mobility of base metals under acidic conditions, thereby enhancing the potential for metal contamination in surrounding water bodies (Gammons et al., 2015). The geochemical impacts of AMD can persist for thousands of years, often requiring complex mitigation strategies to reduce the transport of contaminants in both surface water and groundwater systems (Perez et al., 2010). Consequently, contamination of water resources due to AMD is considered one of the major contributors to water pollution in mining regions (Wang et al., 2021). The overall groundwater quality in mining areas is influenced not only by coal mining activities themselves (Wellen et al., 2018) but also by the interactions between groundwater and surrounding geological formations, which are further intensified under acidic environmental conditions (Anim-Gyampo et al., 2019; Prathap & Chakraborty, 2019).

In many mining regions, understanding the movement and transport of heavy metal contaminants associated with Acid Mine Drainage (AMD) requires detailed knowledge of groundwater recharge sources, groundwater–surface water interactions, and the contribution of atmospheric precipitation to groundwater recharge. These factors are essential for identifying the sources and pathways of groundwater because isotopic components present in water molecules can provide valuable information about hydrological processes (Ali. et al., 2017; Liu et al., 2022). Such information also helps in understanding the interactions between surface water and groundwater systems.

Groundwater recharge occurs through both natural and anthropogenic processes. Natural recharge primarily takes place when precipitation, such as rain or snow, infiltrates the soil, percolates through the unsaturated zone, and eventually reaches the water table. In addition, surface water bodies such as rivers, streams, lakes, and wetlands can contribute to groundwater recharge through seepage from the surface into underlying aquifers (Li et al., 2018; Guan et al., 2019).

Pakistan is currently facing a significant energy crisis, and coal is widely recognized as an important energy resource in the country. Coal is utilized in various sectors, including sugar and steel mills, cement industries, brick kilns, household heating, and power generation for municipal utilities (Khan et al., 2020). Pakistan possesses approximately 90 billion tons of coal reserves, of which about 97% is lignite and the remaining 3% ranges from sub-bituminous to bituminous in rank (Khan et al., 2020).

The present research was conducted in an active mining area at the Pail–Padhrar coal mine site. Previous studies in this region have investigated the adverse impacts of mining activities on groundwater quality; however, these investigations were primarily limited to the assessment of groundwater chemistry (Aniqa et al., 2018; Syed et al., 2015). Comprehensive hydrogeological studies focusing on geochemical processes, the sources of elevated sulfate concentrations, and the potential influence of Acid Mine Drainage (AMD) using isotopic techniques integrated with hydrogeochemical data have not yet been carried out in this mining area. Therefore, this study applies a combination of isotope analysis and hydrogeochemical tools to identify groundwater recharge sources, evaluate the impact of AMD, and distinguish between anthropogenic and geogenic contributions to the elevated concentrations of dissolved salts in groundwater.

Materials and methods

Study area

The study site is located near the area of Choa Saidan Shah in District Chakwal, Punjab, Pakistan (Fig. 1). The Chakwal region hosts approximately 388 mineral mines, including about 246 coal mines with an estimated reserve of nearly 75 million tons. The coal reserves of the Pail–Padharar coalfield, located within the Padharar zone of the Chakwal region, are associated with the Patala Formation and are estimated to contain approximately 63.83 million tons of coal (Shah et al., 2005). The coal deposits occur in the upper part of the Paleocene-aged Patala Formation, which is stratigraphically bounded by the Nammal Formation above and the Lockhart Formation below. The Patala Formation mainly consists of carbonaceous shale interbedded with coal seams and carbonate rock units (Malkani & Malik, 2018).

The upper zone of the aquifer primarily comprises dark grey shale and marl, with minor occurrences of yellowish-brown sandstone and white nodular limestone interbedded within the sequence. The upper stratigraphic section generally consists of greyish-green to brownish-grey shale, grey limestone, and light grey siltstone, whereas the lower section is dominated by thick, well-consolidated sandstone beds forming prominent cliff structures. The thickness of coal seams varies across the area, and in some locations the seams are replaced by clay or sandstone units. The coal rank in the region ranges from lignite to sub-bituminous. Groundwater in the area occurs within discontinuous aquifers in certain parts of the formation (Ibrahim, 2009).

The climate of the study area exhibits considerable seasonal variation. Winters are generally cool and moderately humid, accompanied by light to moderate rainfall, whereas the spring and summer seasons are typically hot and dry. Summers are relatively short but extremely hot and humid, followed by the monsoon season. In contrast, winters are short, cold, and mostly dry. The average annual temperature ranges from

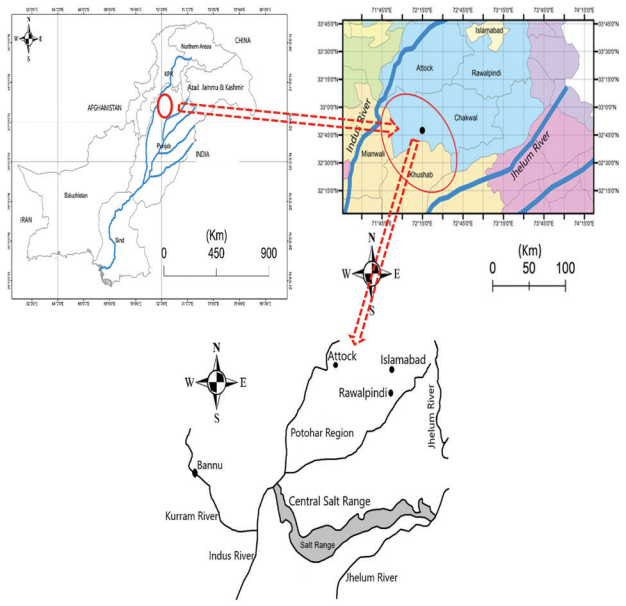

Fig. 1 - Location of study area.
Fig. 1 - Ubicazione dell'area di studio.

approximately 1 °C to 37 °C, rarely dropping below –1 °C or exceeding 41 °C. The mean annual rainfall in the Pail–Padharar region is about 370 mm (14.57 inches).

Sampling and water chemical and isotopes analyses

Water samples were collected from groundwater, mine water, and surface water sources in the study area in collaboration with the Punjab Mineral Development Corporation (PUNJMIN). Sampling sites included mine sumps, pre-existing boreholes, and nearby surface water bodies. For boreholes, prior to sample collection, purging was performed by removing at least three well volumes to ensure that the samples were representative of the aquifer rather than stagnant water in the casing. Water samples were filtered in filed through 0.45 µm membrane filters to remove suspended solids and for cations analysis samples (samples were acidified infield to pH 1–2 using hydrochloric acid (10%)). During collection, transport, and storage, special care was taken to prevent isotope fractionation due to evaporation, diffusion, or interaction with container materials, following IAEA guidelines (IAEA, 2007). Each sample was labeled with a waterproof marker indicating project code, location, date, and sample number, and the information was cross-referenced with field notes. All water samples were stored at low temperatures (4–6 °C) to prevent microbial growth, chemical alteration, or isotopic fractionation prior to laboratory analysis. Sampling campaigns were conducted in September 2021 (post-monsoon), June 2022 (pre-monsoon), and August 2023 (post-monsoon).

Field parameters, including pH, electrical conductivity (EC), and dissolved oxygen (DO), were measured in situ using portable meters. Major cations (Na^+, K^+, Mg^{2+}, Ca^{2+}) and trace metals (Zn, Cd, Pb, Cu, Fe) were analyzed using standard procedures, while major anions (Cl^-, HCO_3^-, CO_3^{2-}, SO_4^{2-}) were determined through titrimetric or ion chromatography methods. Isotopic analyses of $\delta^{18}O$, $\delta^{2}H$, $\delta^{34}S$, and $\delta^{13}C$ were performed to investigate groundwater recharge sources, evaporation effects, and the influence of Acid Mine Drainage (AMD) on water chemistry. The correlation between the Ca^{2+} and SO_4^{2-} is used in the study as the milli-equivalent ratio of Ca^{2+} and SO_4^{2-} equal to 1 indicates that the main origin of SO_4^{2-}, Ca^{2+}, originating from the dissolution of gypsum and anhydrite as shown by following equations.

$$CaSO_4 \cdot H_2O\ (Gypsum) \rightarrow Ca^{2+} + SO_4^{2-} + 2H_2O$$

$$CaSO_4\ (Anhydrite) \rightarrow Ca^{2+} + SO_4^{2-}$$

Furthermore, when iron is introduced into the natural water, it becomes hydrolyzed and forms precipitate of iron hydroxide. Iron in coal mines normally results from pyrite contents in the coal as suggested by other researchers (Aju et al., 2022).

$$FeS_2 + O_2 + H_2O \rightarrow Fe(OH)_3 + 2SO_4^{2-} + 4H^+$$

Chloroalkaline indices (CAI) is applied to is calculated to find ions exchange phenomenon by using following equation (Schoeller; 1965).

$$CAI = Cl^- - (Na^+ + K^+)/\ Cl^-$$

To ensure data reliability, rigorous Quality Assurance (QA) and Quality Control (QC) measures were implemented. These included the use of standard reference materials, procedural blanks, and duplicate samples for all analyses. Instrument calibration was regularly performed using certified standards, and precision was verified through repeated measurements. Laboratory analytical uncertainties were quantified, and all data were cross-checked for consistency and reproducibility before interpretation.

This comprehensive methodology provided a reliable dataset to evaluate hydrochemical facies, water–rock interactions, mineral dissolution, evaporation, and AMD-related geochemical processes in the Pail–Padhrar mining area. In groundwater systems, minimal isotopic fractionation occurs during sulfate release from mineral dissolution or sulfide oxidation, so $\delta^{34}S$ values reliably reflect the source mineral (Seal, 2006). Minor fractionations are typically observed when the net rate of sulfate reduction exceeds the overall sulfur redox turnover (Bottrell et al., 2006). During pyrite oxidation, H_2S may be partially immobilized in metal sulfides according to the reaction:

$$4SO_2 + 4H_2O \rightarrow 3HSO_4^- + 3H^+ + H_2S$$ (Rye et al., 1981)

The sampling points are shown in Figure 2 and co-ordinates are provided in Table 1.

The cations were measured by an atomic absorption spectrometer (Thermo scientific iCe 3000 series). Chloride ions analyzed by argentometric method and sulfate ions determined by UV-visible spectrophotometer (Hitachi 2A) (Frenzel & Michalski, 2016). Total metal concentration was measured by ICP-OES (Thermo Scientific iCAP 6000 series, UK) and by Polarograph (797 Computrace Metrohm). The instruments were calibrated by the standards provided with

Tab. 1 - Sample information: Pail-Padhrar Site.

Tab. 1 - Informazioni dei campioni raccolti nel sito di Pail-Padhrar.

Sample Code	Co-ordinates		Depths (m)
PRW-RW	32°38'39.40"N	72°28'46.3"E	Rain water sample
PCP-1 MW	32°37'54.40"N	72°30'56.80"E	137.0
PCP-3 MW	32°37'36.80"N	72°31'35.70"E	142.0
PCP-4 MW	32°37'15.80"N	72°32'55.00"E	118.0
PCP-4 GW	32°37'14.37"N	72°32'58.50"E	121.0
PCP-5 MW	32°37'55.60"N	72°31'16.70"E	121.0
PCP-6 MW	32°37'23.7"N	72°31'46.5"E	45.0
PCP-7 MW	32°37'56.1"N	72°31'15.90"E	40.0
PCP-8 MW	32°37'34.9"N	72°31'38.8"E	30.0
PM-1 MW	32°37'34.80"N	72°32'42.70"E	135.0
PM-1 GW	32°37'34.80"N	72°32'42.70"E	91.0
PM-2 GW	32°37'0.40"N	72°32'1.90"E	109.0
PM-3 GW	32°36'59.95"N	72°32'3.26"E	115.0
PM-4 GW	32°38'0.30"N	72°29'47.90"E	106.0
PM-5 SW	32°38'51.00"N	72°29'33.00"E	SW
PM-7 GW	32°38'39.40"N	72°28'41.20"E	45.0
PM-8 GW	32º36'49.9" N	72º32'04.6" E	109.0
PM-9 GW	32º38'28.1" N	72º29'47.4" E	60.0
PM-10 GW	32º38'27.48" N	72º29'48.7" E	89.0
PM-11 GW	32º38'31" N	72º29'45.9" E	76.2
PM-12 GW well	32º38'14.7" N	72º29'37.6" E	39.0
PM-13 GW	32º39'4.7" N	72º29'39.4" E	54.0
PM-14 GW	32º38'55.8" N	72º29'33.6" E	82.0
PM-15 GW	32º38'56.67" N	72º29'31.34" E	109.0
PM-16 GW	32º39'3.2" N	72º29'12.3" E	67.0
PM-17 GW	32º38'50.4" N	72º28'50.3" E	91.0
PM-18 GW	32º38'55.5" N	72º29'51.4" E	32.0
PM-19 GW	32º38'57.7" N	72º29'51.6" E	40.0
PM-20 GW	32º39' 01.1" N	72º29'51.4" E	45.0
PM-21 GW	32º39' 02.1" N	72º29'51.8" E	15.0
PM-22 GW	32º38' 43.5" N	72º29'40.6" E	120.0
PM-23 GW	32º39' 01.9" N	72º29'54.1" E	33.0
PM-24 GW	32º38' 50.1" N	72º29'47.9" E	12.0
PM-25 GW	32º38' 49.5" N	72º29'27.7" E	100.0
PM-26 GW	32º38' 49.8" N	72º29'27.9" E	100.0
PM-29 GW	32º38' 19.5" N	72º29'23.3" E	100.0
PM-30 GW	32º39' 21.5" N	72º29'15.8" E	100.0
PM-31 GW	32º39' 21.0" N	72º29'20.8" E	90.0
Where: MW: Mine water; GW: Groundwater; SW: Surface water; RW: Rainwater			

instruments. Detection limits and standard deviation/error of analysis of isotopes (Table 2) and major cations, anions and metals are given in Tables 3a and 3b. Geochemical analysis of the water samples was carried out using graphical methods including the Wilcox Diagram, Piper Diagram, and Gibbs Diagram. The Piper diagram was used to identify hydrochemical facies and dominant water types, while the Gibbs diagram helped to determine the natural processes controlling water chemistry. The Wilcox diagram was applied to assess the suitability of groundwater for irrigation purposes. These graphical tools provided insight into the geochemical evolution and quality of groundwater in the study area.

Water samples were analyzed for stable isotopes, including $\delta^{18}O$ and $\delta^{2}H$, to investigate groundwater recharge sources,

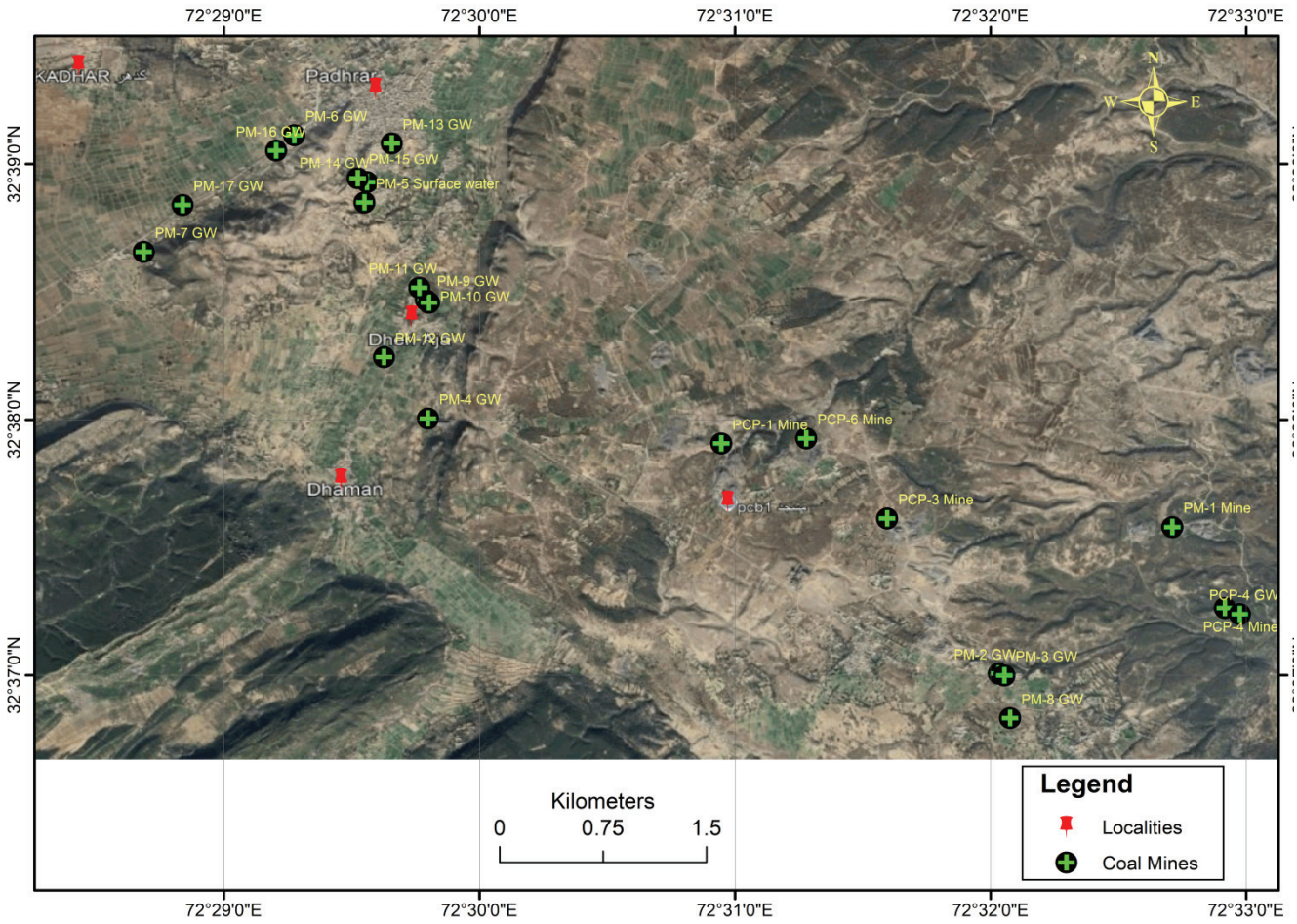

Fig. 2 - Sampling points in study area.

Fig. 2 - Punti di campionamento nell'area di studio.

evaporation effects, and hydrogeochemical processes. Selected samples with sufficiently high sulfate concentrations were further analyzed for $\delta^{34}S$ and $\delta^{18}O$ of sulfate to trace the sources and processes controlling sulfate in groundwater. The $\delta^{18}O/\delta^{2}H$ ratios of water samples were measured using the CO_2 equilibration method, in which water equilibrates with CO_2 under controlled conditions, allowing the oxygen isotope ratio to be determined (Drost & Klotz, 1983). For $\delta^{2}H$ analysis, hydrogen gas (H_2) was generated from water using the zinc reduction method (Halevy, 1967), and the $^{2}H/^{1}H$ ratio of the gas was measured using an isotope ratio mass spectrometer (IRMS) (Klotz, 1978).

Sulfate isotopes ($\delta^{34}S$ and $\delta^{18}O$) were analyzed after precipitation of sulfate as barium sulfate ($BaSO_4$). Samples were acidified to pH 1–2 with hydrochloric acid (10%), and $BaCl_2$ solution (5–6 mL of 20%) was added to precipitate sulfate. The precipitate was thoroughly rinsed with distilled water until neutral, dried, and homogenized. Approximately 0.3 mg of $BaSO_4$ was converted to SO_2 in an elemental analyzer for sulfur isotope measurement, and to CO in a pyrolysis reactor for oxygen isotope measurement, followed by IRMS analysis. The CDT reference materials used for normalization for sulfur isotopes. The overall analytical errors ±0.1‰ ($\delta^{34}S$) were recorded for measurements.

All isotope data are expressed in δ‰ relative to the Vienna Standard Mean Ocean Water (VSMOW) for $\delta^{18}O$ and $\delta^{2}H$, and to standard reference materials for $\delta^{34}S$. The overall analytical errors were ±0.01‰ for $\delta^{18}O$ and $\delta^{2}H$, and ±0.1‰ for $\delta^{34}S$. Stable isotope measurements were performed using a Varian MAT GD-150 mass spectrometer. Quality assurance and quality control measures included the use of standard reference materials, repeated measurements, and calculation of standard deviations to ensure precision and reproducibility of the isotopic data.

Isotope ratio (δ‰) of $\delta^{15}N$, $\delta^{2}H$ and $\delta^{18}O$ were calculated by using following relation:

$$\delta‰\ Vs\{std\}=\{R_{sample}/R_{std}-R_{std}/R_{std}\}(1000\ \delta‰)$$

The overall analytical errors ± 0.01 ‰ ($\delta^{2}H$ and $\delta^{18}O$) were recorded for measurements. To ensure precision, the standard deviation of the mass spectrometer has computed and the standard deviation of each sample was ensured to be within the permissible limit. The values of d-excess were calculated by:

$$d\text{-}excess = \delta D - 8\delta^{18}O$$

Results

Stable isotopes analysis

The Local Meteoric Water Line (LMWL) was established using the slope and intercept derived from isotopic analysis of rainwater samples collected throughout the year, covering both pre-monsoon and post-monsoon seasons. This approach provided comprehensive isotopic information to identify potential groundwater recharge sources. The average, minimum, and maximum values of $\delta^{18}O$, $\delta^{2}H$, and d-excess for groundwater, mine water, surface water, and rainwater from all three sampling campaigns are presented in Table 2.

Hydrochemical characteristics

The samples were analyzed for major cations, anions and metals in the groundwater, mine water and rainwater samples. It is observed that in Pail-Padhrar area concentration of major cations in mine water samples ranges as: Ca^{2+} (ppm): from 20.0 to 158.0 (avg. 72.0±7.9); Mg^{2+} (ppm): 0.0 to 21.0 (Avg. 2.0±0.1) Na^{+} (ppm): 21.0 to 908.0 (Avg. 228.0±11.9); K^{+} (ppm): 1.0 to 8.0 (Avg. 3.0±0.1). Whereas as the concentration of major cations in groundwater water samples ranges as: Ca^{2+} (ppm): from 20.0 to 216.0 (avg. 77.0±3.6); Mg^{2+} (ppm): 0.0 to 35.0 (Avg. 4.0±0.2); Na^{+} (ppm): 14.0 to 5221.0 (Avg. 576.0±8.3); K^{+} (ppm): 1.0 to 32.0 (Avg. 6.0±1.2).

The concentration of major anions in mine water samples ranges as: Cl^{-}(ppm): from 20.0 to 84.0 (avg. 34.0±1.1); CO_3^{-}(ppm): 0.0 to 48.0 (Avg. 5.0±0.6); HCO_3^{-}(ppm): 146.0 to 1080.0 (Avg. 479.0±12.2); SO_4^{-2}(ppm): 23.0 to 836.0 (Avg. 233.0±9.2). Whereas as the concentration of major anions in groundwater water samples ranges as: Cl^{-}(ppm): from 20.0 to 4786.0 (avg. 510.0±3.6); CO_3^{-}(ppm): 0.0 to 24.0 (Avg. 4.0±0.2); HCO_3^{-}(ppm): 397.0 to 775.0 (Avg. 504.0±14.2); SO_4^{-}(ppm): 15.0 to 394.0 (Avg. 64.0±2.3).

The cations and anions in the rainwater samples were also analyzed and the concentration ranges as: Ca (ppm): from 1.0 to 3.0 (avg. 2.0±0.2); Mg (ppm): 1.0 to 3.0 (Avg. 1.0±0.1); Na (ppm): 0.0 to 3.0 (Avg. 1.0±7.9); K (ppm): 0.0 to 4.0 (Avg. 2.0±0.1), whereas the concentration of anions in rainwater samples ranges as: Cl (ppm): from 9.0 to 57.0 (avg. 15.0±7.9); HCO_3 (ppm): 61.0 to 153.0 (Avg. 114.0±10.3); SO_4 (ppm): 5.0 to 12.0 (Avg. 7.0±1.3).

The concentration of metals were also analyzed and the concentration of metals in mine water samples ranges as; Zn (ppm): from 12.0 to 32.0 (avg. 24.0±2.3); Cd (ppm): 0.01 to 0.03 (Avg. 0.01±0.001); Pb (ppm): 17.0 to 29.0 (Avg. 20.0±1.4); Cu (ppm): 16.50 to 17.30 (Avg. 16.90±1.2); Fe (ppm): 0.04 to 0.15 (Avg. 0.09±0.01). The concentration of metals in groundwater samples ranged as follow: Zn (ppm): from 8.0 to 30.0 (avg. 17.0±1.3); Cd (ppm): 0.21 to 0.23 (Avg. 0.22±0.01); Pb (ppm): 6.0 to 29.0 (Avg. 14.0±1.3); Cu (ppm): 8.0 to 20.0 (Avg. 16.0±1.6); Fe (ppm): 0.09 to 0.18 (Avg. 0.14±0.03) .

The cations and anions concentrations in mines water and groundwater are in order as:

Mines water:
(cations) Na > Ca >K> Mg; (anions) HCO_3 > SO_4 > Cl > CO_3

Groundwater:
(cations) Ca >Na > K> Mg; (anions) Cl > HCO_3 > SO_4 > CO_3

Whereas, the metals concentration in mines water and groundwater are in order as:

Mines water: Zn > Pb > Cu > Fe > Cd

Groundwater: Zn > Cu > Pb > Cd > Fe

The average concentration of cations and anions in all three samplings is provided in Table 3a and average concentration of metals is provided in Table 3b.

Tab. 2 - Isotopic values of samples of Pail-Padhrar Site.

Tab. 2 - Valori isotopici dei campioni raccolti nel sito di Pail-Padhrar.

Sampling 1									
Stable isotopes values	Groundwater samples			Mines water samples			Surface water samples		
	$\delta^{18}O$‰ ±0.01 ‰	$\delta^{2}H$‰ ±0.01 ‰	d-Excess	$\delta^{18}O$‰ ±0.01 ‰	$\delta^{2}H$‰ ±0.01 ‰	d-Excess	$\delta^{18}O$‰ ±0.01 ‰	$\delta^{2}H$‰ ±0.01 ‰	d-Excess
Average	-6.51	-37.69	14.42	-6.19	-36.32	13.20	1.7	-3.18	-15.82
Minimum	-6.81	-39.68	11.92	-6.39	-37.20	10.99	1.6	-3.20	-16.21
Maximum	-6.14	-35.01	17.07	-5.76	-35.09	15.33	1.8	-3.16	-15.42
Sampling 2									
Average	-5.45	-34.17	9.47	-5.65	-35.45	9.72	2.3	-3.13	-20.72
Minimum	-6.46	-39.46	3.81	-6.24	-39.20	5.55	2.2	-3.14	-21.30
Maximum	-2.94	-19.41	12.53	-4.73	-32.29	11.72	2.4	-3.12	-20.14
Sampling 3							Rainwater samples		
Average	-6.52	-36.10	16.07	-6.80	-39.51	14.91	-10.30	-68.28	14.16
Minimum	-6.92	-41.08	10.69	-7.1	-41.98	7.46	-12.66	-88.82	11.82
Maximum	-5.33	-15.88	26.76	-5.87	-31.95	17.04	-6.02	-31.84	16.32

Tab. 3a - Concentration of major cations and anions in Pail-Padhrar Site samples.

Tab. 3a - Concentrazione dei cationi e anioni principali per i campioni raccolti nel sito di Pail-Padhrar.

Mines Water samples								
Conc. (ppm)	Ca^{2+} (±1.0)	Mg^{2+} (±0.5)	Na^{+} (±1.0)	K^{+} (±0.5)	Cl^{-} (±1.0)	CO_3^{2-} (±1.0)	HCO_3^{-} (±1.0)	SO_4^{2-} (±1.0)
Min.	20	0	21	1	20	0	146	23
Max.	158	21	908	8	84	48	1080	836
Average	72	2	228	3	34	5	479	233
Groundwater samples								
Conc. (ppm)	Ca	Mg	Na	K	Cl	CO_3	HCO_3	SO_4
Min.	20	0	14	1	20	0	397	15
Max.	216	35	5221	32	4786	24	775	394
Average	77	4	576	6	510	4	504	64
Detection limits (ppm)	0.009	0.003	0.003	0.008	1.00	1.00	1.00	1.00

Tab. 3b - Concentration of metals in Pail-Padhrar Site samples.

Tab. 3b - Concentrazione dei metalli in traccia per i campioni raccolti nel sito di Pail-Padhrar.

Mines Water samples					
Conc. (ppm)	Zn^{2+} (±0.5)	Cd^{2+} (±0.5)	Pb^{2+} (±0.5)	Cu^{2+} (±0.5)	Fe^{3+} (±0.5)
Min.	12	0.01	17	16.50	0.04
Max.	32	0.03	29	17.30	0.15
Average	24	0.01	20	16.90	0.09
Groundwater samples					
Conc. (ppm)	Zn^{2+} (±0.5)	Cd^{2+} (±0.5)	Pb^{2+} (±0.5)	Cu^{2+} (±0.5)	Fe^{3+} (±0.5)
Min.	8	0.21	6	8	0.09
Max.	30	0.23	29	20	0.18
Average	17	0.22	14	16	0.14
Detection limits (ppm)	0.01	0.013	0.073	0.033	0.052

Discussion

Groundwater source identification

The interpretation of isotopic data for recharge mechanisms in the study area was based on control points, including the local meteoric water line, rainwater index, and surface water bodies. Rainwater stable isotopes collected over multiple years were used to construct the Local Meteoric Water Line (LMWL) with the equation $\delta^2H = 7.63 \times \delta^{18}O + 10.26$. For comparison, the Global Meteoric Water Line (GMWL) was plotted as $\delta^2H = 8.0 \times \delta^{18}O + 10$ (Rozanski et al., 1992). Groundwater $\delta^{18}O$ vs δ^2H data indicated that most samples fall marginally along the LMWL (Fig. 3a), suggesting that shallow groundwater is predominantly recharged by local precipitation.

The isotopic composition of precipitation exhibited clear seasonal variation. Pre-monsoon rainfall was enriched in heavier isotopes ($\delta^{18}O$ and δ^2H) due to higher temperatures enhancing isotope fractionation, whereas post-monsoon rainfall showed isotopic depletion associated with intense rainfall events, consistent with the amount effect (Rozanski et al., 1992; 2019).

Enriched $\delta^{18}O$ values in groundwater are attributed to isotopic modification during infiltration and subsurface water–rock interactions. Oxidation of sulfide minerals such as pyrite (FeS_2) during infiltration can induce oxygen isotope exchange between water and sulfur species, further enriching $\delta^{18}O$. Enrichment in $\delta^{18}O$ relative to the MWL, without corresponding changes in δ^2H, suggests oxygen isotope exchange with bedrock minerals (Odri et al., 2020).

Isotopic and hydrochemical analyses indicate that sulfate (SO_4^{2-}) in groundwater originates from multiple sources, including atmospheric precipitation, sulfide mineral oxidation, evaporite dissolution, sewage, and mine drainage (Chunlu et al., 2022). Deviations in $\delta^{18}O$ without significant δ^2H changes may also result from oxygen isotope exchange with dissolved CO_2, mineral dissolution and re-precipitation, or isotopic exchange with surrounding minerals (Ruta et al., 2017). Atmospheric CO_2 may enter groundwater via mixing or diffusion, while CO_2 produced by microbial oxidation of organic matter can equilibrate with groundwater oxygen isotopes (Cartwright et al., 2002). Isotopic plots showing interaction with CO_2 and H_2S further confirm significant groundwater–rock interaction, leading to observed isotopic shifts (Fig. 3b).

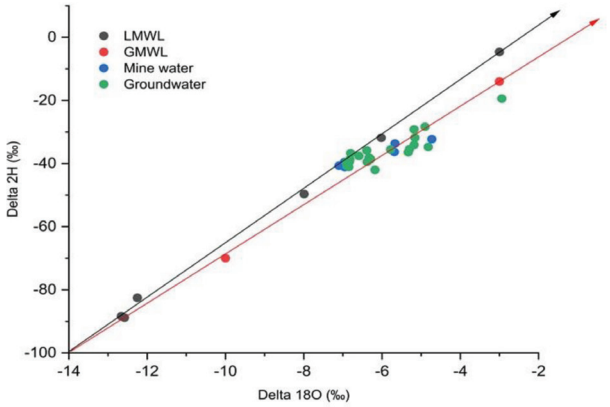

Fig. 3a - Isotopic graph of hydrological samples of Pail-Padhrar Site: samples are lying on evaporation and gasses exchange lines.

Fig. 3a - Grafico della composizione isotopica per i campioni raccolti nel sito di Pail-Padhrar: i campioni si dispongono lungo le linee di evaporazione e di scambio gassoso.

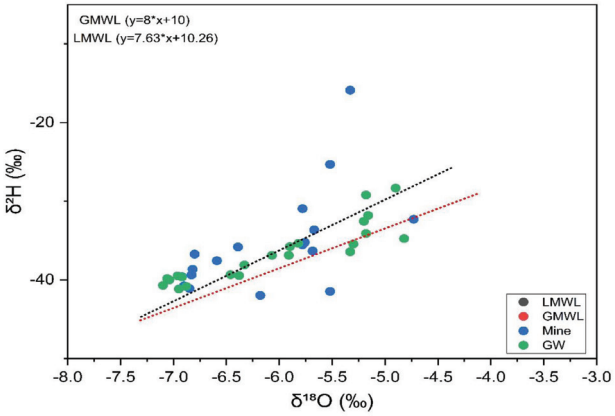

Fig. 3b - Isotopic data showing the gas exchange in groundwater samples; Isotopes exchange with CO_2; hydrocarbons and H_2S gasses.

Fig. 3b - Dati isotopici che mostrano processi di scambio gassoso nei campioni di acque sotterranee, con scambio isotopico con CO_2, idrocarburi e H_2S.

Spatial variation of d - Excess

Deuterium excess (d-excess), defined as $d = \delta^2H - 8\delta^{18}O$, has a value of +10 in the Global Meteoric Water Line (GMWL), indicating that evaporation from continental water bodies under low humidity conditions can produce vapor with elevated d-excess (Dansgaard, 1964). In this study, samples were grouped based on their d-excess and $\delta^{18}O$ values, as summarized in Figure 4.

The relationship between d-excess and $\delta^{18}O$ provides insights into hydrological processes such as mixing, evaporation, and mineral dissolution. During mineral dissolution, d-excess remains largely constant, whereas evaporation causes a decrease in d-excess values (Dansgaard, 1964; Gat, 1996; Qu et al., 2023). The $\delta^{18}O$ value may decrease during mixing with rainwater, remain constant or increase slightly during mineral dissolution, and increase significantly during evaporation (Yang & Han, 2020; Fryar et al., 2021; Qu et al., 2023).

The high variability of d-excess in the collected samples reflects spatial heterogeneity in the unsaturated zone, resulting in variable exposure of infiltrating water to

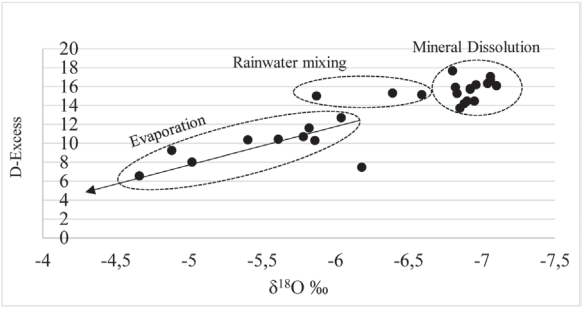

Fig. 4 - Correlation of D-excess and $\delta^{18}O$.

Fig. 4 - Correlazione tra d-excess e $\delta^{18}O$.

fractionation effects associated with evaporation (Fynn et al., 2016). Higher d-excess values in shallow groundwater indicate mixing with rainwater, which carries a distinct isotopic signature, while mineral dissolution in the subsurface also modifies groundwater isotopic composition (Sreedevi et al., 2021). Conversely, lower d-excess values in mine water samples suggest a stronger influence of evaporation (Tianming & Zhonghe, 2012). Intermediate d-excess values observed in shallow groundwater near active mines likely reflect mixing between meteoric water and water impacted by Acid Mine Drainage (AMD) (Thomas et al., 2020). Groundwater samples exhibiting low d-excess and enriched $\delta^{18}O$ indicate varying degrees of evaporation prior to recharge. Relatively lower d-excess values during the post-monsoon period are attributed to significant recharge from rainfall into the shallow aquifer (Bruska et al., 2024).

$\delta^{34}S$ and $\delta^{18}O$ of sulfates

Determination of the sulfur isotopic composition of dissolved sulfate ($\delta^{34}S$) is a valuable tool for identifying sulfate sources in groundwater (Seal, 2006). In particular, the combined analysis of $\delta^{34}S$ and $\delta^{18}O$ of sulfate provides insight into the processes controlling sulfate formation and transport (Böttcher, 2011). In the study area, $\delta^{34}S$ values ranged from –13.7 to 3.04‰ (CDT) (Fig. 5). Isotopic data indicate that dissolved sulfate in acidic mine drainage was primarily derived from the oxidation of pyrite within the coal seams, whereas sulfate in groundwater from the underlying limestone aquifer mainly originated from leaching of gypsum ($CaSO_4$). The gypsum in the aquifer is naturally occurring rather than mine waste–derived, although mine development can accelerate evaporite weathering when local strata contain gypsum, resulting in elevated SO_4^{2-} concentrations and $\delta^{34}S$ values (An et al., 2020; Liu et al., 2017).

The presence of iron oxyhydroxides in groundwater further confirms pyrite oxidation as a source of sulfate. Shallow groundwater samples also contain atmospheric sulfate. Atmospheric deposition, whether wet (rain, snow) or dry (particulate, gaseous), represents an additional sulfate source. Coal-burning industries in the area release significant amounts of SO_4 into the atmosphere, which subsequently contributes sulfate to precipitation. Rainwater in the region

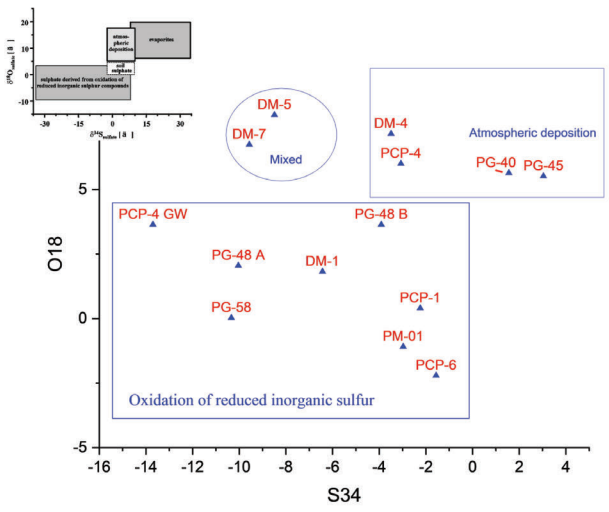

Fig. 5 - $\delta^{34}S$ ‰ and $\delta^{18}O$ ‰ of sulfates in groundwater, suggesting sources of sulfates.

Fig. 5 - $\delta^{34}S$ ‰ e $\delta^{18}O$ ‰ presente nei solfati nei campioni di acque sotterranee, indicativi dell'origine dei solfati.

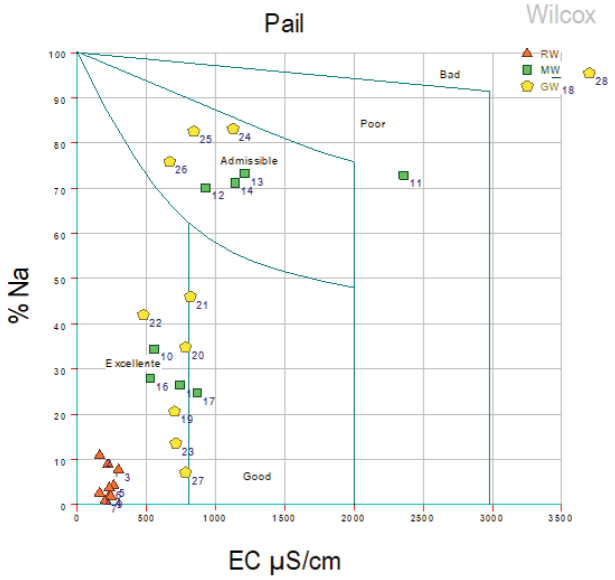

Fig. 6 - Wilcox Diagram of Pail area.

Fig. 6 - Diagramma di Wilcox relativo all'area di Pail-Padhrar.

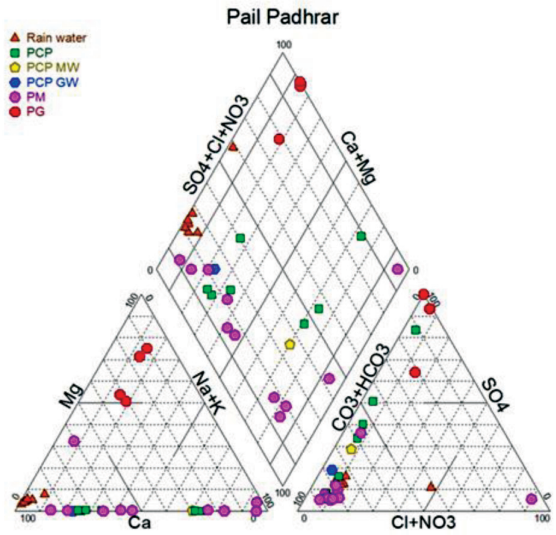

Fig. 7 - Piper Diagram of Pail-padhrar area.

Fig. 7 - Diagramma di Piper relativo all'area di Pail-Padhrar.

contains sulfate concentrations of 6-10 mg/L, which infiltrates the unsaturated zone and mixes with shallow groundwater. In some samples, sulfate isotopic composition indicates mixing of sources from both geology and atmospheric deposition, consistent with a well-connected surface water–groundwater system, as corroborated by stable isotope data.

Overall, four major sources of sulfate were identified in the study area: (i) pyrite oxidation, (ii) dissolution of sulfate minerals (e.g., gypsum), (iii) atmospheric deposition, and (iv) residual or recycled sulfate from previous reduction and re-oxidation.

Geochemical data

Geochemical data suggest the acidic nature of mine water, while the groundwater samples are neutral to alkaline in nature. High level of EC, TDS, chloride, sulfates and major cations in the samples shows that majority of groundwater samples are suitable for drinking purposes as these are in the range of good quality limits. Few groundwater samples (mostly shallow) are in bad quality range as shown in Wilcox diagrams (Wilcox, 1955) (Fig. 6).

Piper diagram (Piper, 1953) revealed two hydrochemical facies, SO_4^{2-}-Cl^--Na^+-Ca^{2+} and HCO_3^--Na^+-Ca^{2+} types. Whereas Na^+ and Ca^{2+} were dominant cations, HCO_3^-, SO_4^{2-} and Cl^- were dominant anions (Fig. 7).

Hydrochemical analysis of groundwater in the study area indicates that water–rock interactions are the primary control on water chemistry, with evaporation playing a secondary role. The Gibbs diagram (Gibbs, 1970) shows that most groundwater samples fall within the rock weathering-dominated field, while a few plot in the evaporation zone, highlighting the influence of both lithology and climatic conditions (Fig. 8). Complementing this, the Piper diagram (Piper, 1953) identifies two main hydrochemical facies: SO_4^{2-}–Cl^-–Na^+–Ca^{2+} and HCO_3^-–Na^+–Ca^{2+}. Among the cations, Na^+ and Ca^{2+} are dominant, whereas HCO_3^-, SO_4^{2-}, and Cl^- are the major anions. These results collectively suggest that groundwater chemistry in the Pail–Padhrar area is largely governed by water–rock interactions, mineral dissolution, and secondary processes such as evaporation, consistent with the influence of local geology and hydroclimatic conditions.

The ration between the pH and molar ratio of HCO_3^-/HCO_3^- + SO_4^{2-} is a good tool to understand the rock-water interaction. The molar ratio of HCO_3^- to (CO_3^{2-} + SO_4^{2-}) further elucidates water–rock interactions. Ratios greater than 0.5 indicate dominance of carbonate reactions, while ratios below 0.5 reflect sulfide oxidation, primarily from pyrite (Kumar et al., 2022). Samples with ratios around 0.5 represent a combination of carbonate dissolution and

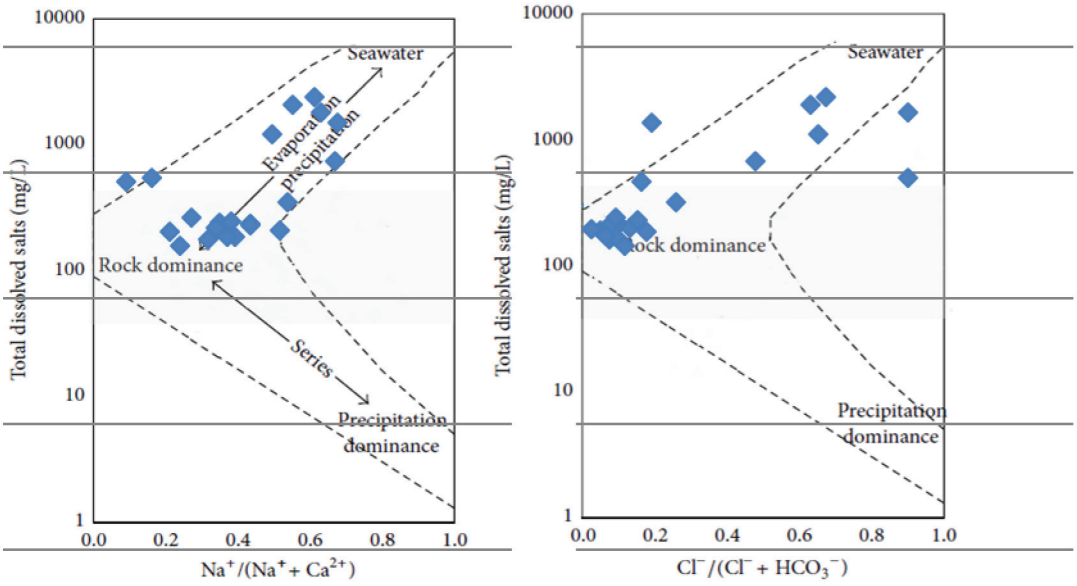

Fig. 8 - Gibbs Diagram.

Fig. 8 - Diagramma di Gibbs.

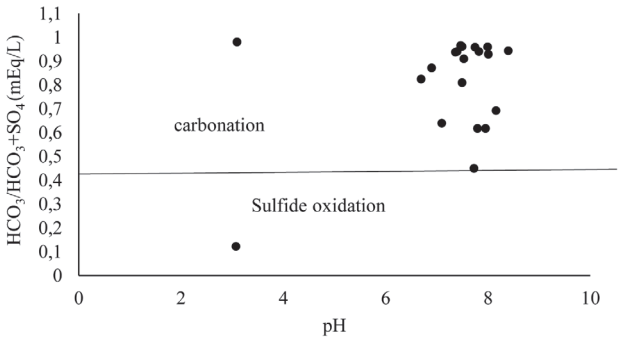

Fig. 9 - Correlation of pH and $HCO_3^-/HCO_3^-+SO_4^{2-}$ showing carbonation processes as dominant phenomenon in groundwater samples.

Fig. 9 - Correlazione tra pH e $HCO_3^-/HCO_3^-+SO_4^{2-}$ che evidenzia i processi di carbonatazione come il fenomeno dominante nei campioni di acque sotterranee.

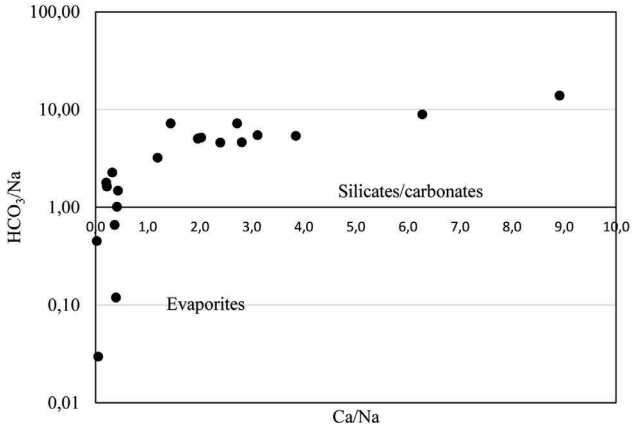

Fig. 10 - Correlation between the ratios of Ca^{2+}/Na^+ and HCO_3^-/Na^+ showing dissolution of evaporates along with silicates and carbonates dissolution in groundwater samples.

Fig. 10 - Correlazione tra i rapporti Ca^{2+}/Na^+ and HCO_3^-/Na^+ indicativa di processi di dissoluzione delle evaporiti, nonché di silicati e carbonati, nei campioni di acque sotterranee.

sulfide oxidation (Fig. 9). Both processes generate protons that enhance the weathering of carbonates, silicates, and other minerals. In the study area, most deep groundwater samples are controlled by carbonation processes, whereas shallow groundwater near mine sites is influenced by pyrite oxidation. This oxidation produces additional protons, intensifying mineral dissolution and contributing to elevated sulfate and TDS concentrations, consistent with AMD impacts. Overall, groundwater chemistry in the region reflects a combination of natural geochemical processes and anthropogenic influences from mining activities, with water–rock interactions as the dominant controlling factor (Li et al. 2018).

The correlation between the molar ratios of Ca^{2+}/Na^+ and HCO_3^-/Na^+ (Fig. 10) provides an additional indicator of mineral dissolution processes. Samples with ratios greater than 1 suggest dominance of carbonate and silicate dissolution, whereas samples with ratios below 1 indicate the dissolution of evaporite minerals (Belkhiri et al., 2012).

The most dominant dissolution of evaporates included the dissolution of halite. The sources of Na^+ and Cl^- ions can be recognized by the ratio of Na^+/Cl^-. In case of halite dissolution, the points would be placed on or near 1:1 line (Roy et al., 2020). In our data few points are placed on or near the 1:1 line and most of points are blow the 1:1 line it indicates high molar concentration of Na^+ as compared to Cl^-as shown in Figure 11. This high molar concentration of Na may be attributed to ion exchange process in the hydrological system.

Chloroalkaline indices (CAI) proposed a significant ion exchange phenomenon in the study area.

Data suggested that the CAI values are positive for all water samples in the study area. When Na^+ and K^+ in the groundwater system exchange with Mg^{2+} or Ca^{2+}, CAI values

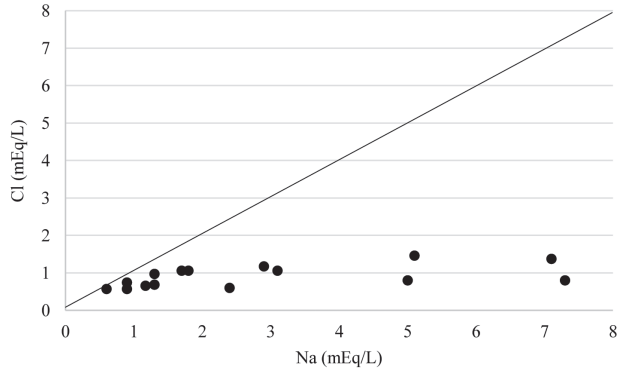

Fig. 11 - Correlation between Na^+ and Cl^- ions showing NaCl as main dissolved evaporates in aquifer.

Fig. 11 - Correlazione tra ioni Na^+ e Cl^- che mostra NaCl come il principale contributo evaporitico disciolto nell'acquifero.

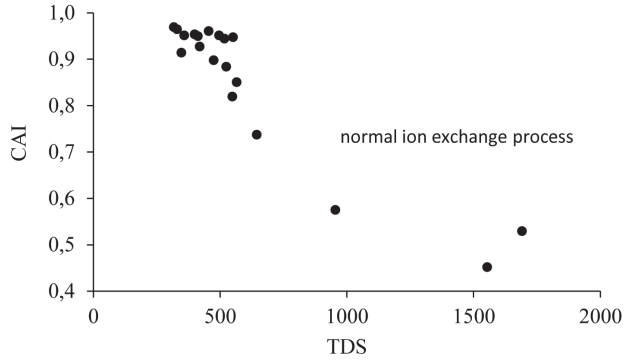

Fig. 12 - Correlation between CAI and TDS showing normal ion exchange is main phenomenon alongside reverse ion exchange.

Fig. 12 - Correlazione tra CAI e TDS che mostra la predominanza dello scambio ionico normale, associato anche a processi di scambio ionico inverso.

are positive. In this system, Na^+ and K^+ ions are replaced by Ca^{2+} ions resulting in a decrease in concentration of these ions groundwater, representing a normal ion exchange process or direct ion exchange (Zongjun et al., 2019) as shown in Figure 12. This findings were also supported by considering the ratio of Ca^{2+}/Na^+ ions. The ratio in most of samples were more than 1, suggesting the significantly higher concentration of Ca^{2+} as compared to sodium in the water samples of study area.

The possible contribution of gypsum in geological system towards the high concentration of sulfate was also elucidated by developing a correlation between the Ca^{2+} and SO_4^{2-} ions. This plot (Fig. 13) deduces the contribution of gypsum and/or anhydrite dissolution as it contributes to an equal amount of Ca^{2+} and SO_4^{2-} in the hydrological samples.

The samples placed on line suggested the gypsum dissolution whereas the samples placed above the equiline suggested the oxidation of pyrite as major source of sulfates in the water groundwater samples (Equeenuddin et al., 2010). Whereas, the samples placed under the 1:1 line suggested the dissolution of carbonates/silicates (Roy et al., 2020) and cation exchange processes decreasing the Ca^{2+} ions (Ali et al. 2023). The oxidation of pyrites also supported by the facts that most of water samples collected from mines showed yellow colored precipitates after exposure to air. The yellowish color of water

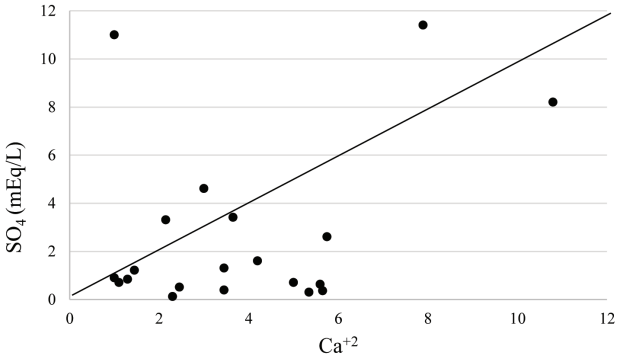

Fig. 13 - Correlation of Ca^{2+} and SO_4^{2+}.

Fig. 13 - Correlation of Ca^{2+} e SO_4^{2+}.

is likely due to the formation of iron hydroxide [$Fe(OH)_3$], which is commonly found in the water bodies near coal mining areas.

The sulfur bearing minerals like pyrites during mining process, exposed to air (oxidized) and water leads to generate the acid mine drainage (AMD) as the result of sulfide oxidation. In effect, sulfide oxidation in the mining environment not only leads to the decrease of pH in the water, but it also increases the sulfate content in the receiving water and accelerate the dissolution of carbonate

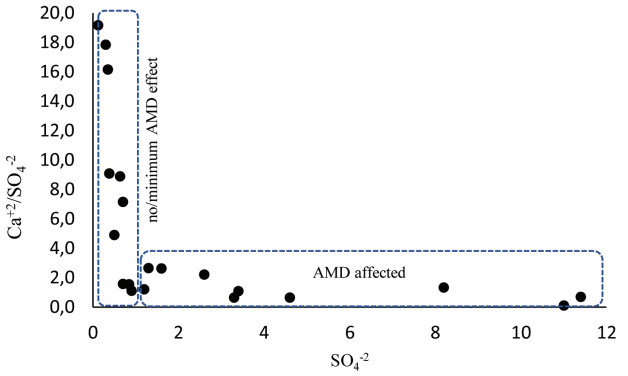

Fig. 14 - Correlation between the molar ratio of Ca^{2+}/SO_4^{2+} and SO_4^{2+}.

Fig. 14 - Correlazione tra rapporto molare di Ca^{2+}/SO_4^{2+} e SO_4^{2+}.

rocks. Untreated AMD released in open pits is a matter of concern as its seepage elicits the geological process in unsaturated zone. The impact of AMD was studied by using the correlation between the molar ratios of Ca^{2+}/SO_4^{2-} and SO_4^{2-} (Spangenberg et al., 2007). Samples are placed in the area of both AMD affected and with minimum AMD affects (Fig. 14). Most of groundwater samples collected from mining activities areas were AMD affected samples whereas the samples collected from vicinity of mining areas were not significantly affected by AMD. Furthermore, the shallow groundwater samples have more AMD impacts than deep groundwater samples.

The pyrite oxidation reaction in hydrological system might affects the δ^2H and $\delta^{18}O$ values. The oxidation of pyrites might lead to enriched $\delta^{18}O$ values. As a result, sulfates and oxides produced with enriched $\delta^{18}O$ values, can cause a shift

in $\delta^{18}O$ values in AMD and AMD-impacted relative to water with no/and or negligible AMD impacts. The Figures 15a and 15b, illustrates the samples having AMD impacts and vice versa. These graphs supports the conclusion that in the study area both gypsum dissolution and pyrite oxidation processes are responsible for the high concentration of SO_4^{2-} in the groundwater samples.

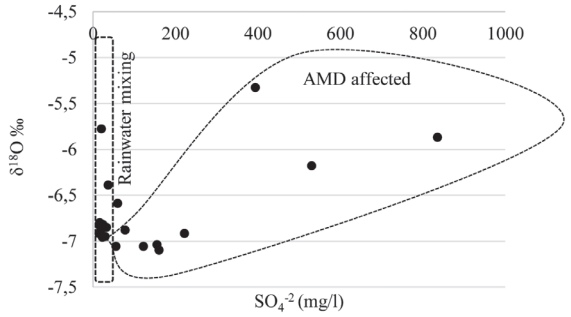

Fig. 15a - Correlation between $\delta^{18}O$ (‰) and SO_4^{2+}.

Fig. 15a - Correlazione tra $\delta^{18}O$ (‰) and SO_4^{2+}.

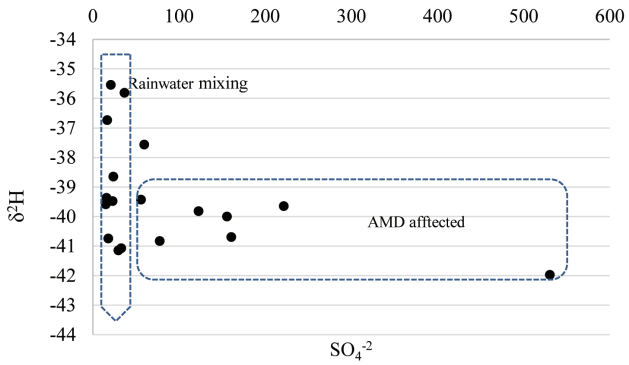

Fig. 15b - Correlation between $\delta^{2}H$ (‰) and SO_4^{2+}.

Fig. 15b - Correlazione tra $\delta^{2}H$ (‰) e SO_4^{2+}.

Conclusions

Stable isotope and hydrogeochemical analyses were conducted in the active Pail–Padhrar mining area, Chakwal, Pakistan, to evaluate the factors controlling Acid Mine Drainage (AMD) impacts on groundwater chemistry. The results indicated spatial variability in AMD influence: some locations showed strong AMD effects, while others were largely unaffected. AMD-impacted water was characterized by a SO_4^{2-}–Cl^-–Na^+–Ca^{2+} hydrochemical type, with high TDS, low pH, and water chemistry dominated by sulfide oxidation, evaporation, and secondary silicate weathering. Non-AMD-affected water exhibited SO_4^{2-}–Na^+–Ca^{2+} to Na^+–Ca^{2+}–HCO_3^- or mixed hydrochemical types, controlled primarily by rock weathering, mineral dissolution, evaporation, and ion exchange.

Stable isotope signatures ($\delta^{2}H$ and $\delta^{18}O$) indicated that most groundwater was recharged by local precipitation, whereas a few depleted samples reflected contributions from evaporated surface water. In AMD-impacted waters, isotopic data suggested that evaporation and mineral dissolution were dominant, with minor effects from rainwater mixing. D-excess values indicated prevailing mineral dissolution in groundwater, dominant evaporation in mine waters, and intermediate values reflecting AMD influence. Sulfate isotopes ($\delta^{34}S$ and $\delta^{18}O$) and geochemical data revealed that groundwater sulfate was primarily sourced from pyrite oxidation, with additional contributions from gypsum dissolution. The presence of iron oxyhydroxides further supported pyrite oxidation. High variability in $\delta^{18}O$, $\delta^{2}H$, and d-excess among samples reflected spatial heterogeneity in infiltration rates and isotope fractionation during recharge.

Competing interest
The author declare no competing interest.

Funding source
The author declares that no funding was received for this study.

AI Use Declaration Statement
The author declares here that paper is produced by author himself without using AI tools.
Only chatgpt is used to improve the grammar of text on few points.

Additional information
DOI: https://doi.org/10.7343/as-2026-966
Reprint and permission information are available writing to acquesotterranee@anipapozzi.it
Publisher's note Associazione Acque Sotterranee remains neutral with regard to jurisdictional claims in published maps and institutional affiliations.

REFERENCES

Aju, C.D., Reghunath, R., Achu, A.L., Rajaneesh, A. (2022). Understanding the hydrogeo-chemical processes and physical parameters controlling the groundwater chemistry of a tropical river basin, South India. Environmental Science and Pollution Research. 29 (16), 23561–23577. DOI:10.1007/s11356-021-17455-w.

Ali, J., Kazi, T. G., Tuzen, M., Ullah, N. (2017). Evaluation of mercury and physicochemical parameters in different depths of aquifer water of Thar coalfield, Pakistan. Environmental Science and Pollution Research, 24(21), 17731–17740. https://doi.org/10.1007/s11356-017-9291-z.

Ali, A., Aissam, G., Hani, A. A., Juris, B., Selma, B., Ivar, Z., Andrey, E. K. (2023). Chemometrics of the environment: hydrochemical characterization of groundwater in Lioua Plain (North Africa) using time series and multivariate statistical analysis, Sustainability, 15, 20. https://doi.org/10.3390 /su15010020.

An, S., Jiang, C., Zhang, W., Chen, X. and Zheng, L. (2020). Influencing factors of the hydrochemical characteristics of surface water and shallow groundwater in the subsidence area of the Huainan Coalfield. Arabian Journal of Geosciences, 13, 1-11.DOI:10.1007/s12517-020-5140-3.

Anim-Gyampo, M., Anornu, G. K., Appiah-Adjei, E. K., & Agodzo, S. K. (2019). Quality and health risk assessment of shallow groundwater aquifers within the Atankwidi basin of Ghana. Groundwater for Sust. Develop. 9, 100217. https://doi.org/10.1016/j.gsd.2019.100217.

Aniqa, B., Sadia, A., Saima, I., Syeda, S. K., Mateen, S., Muhammad, A. G. (2018). Physico-chemical quality of drinking water and human health: a study of salt range Pakistan. International Journal of Hydrology, 2(6), 668-677. DOI:10.15406/ijh.2018.02.00141

Belkhiri, L., Mouni, L., Boudoukha, A. (2012). Geochemical evolution of groundwater in an alluvial aquifer: case of El Eulma aquifer, East Algeria. Journal of African Earth Sciences, 66, 46–55. DOI:10.1016/j.jafrearsci.2012.03.001.

Bian, Z., Inyang, H. I., Daniels, J. L., Otto, F., Struthers, S. (2010). Environmental issues from coal mining and their solutions. Mining Science and Technology, 20(2), 215–223. https://doi.org/10.1016/S1674-5264(09)60187-3.

Bottcher, M.E. (2011). In: Reitner, J., Dordrecht, Thiel V. (Eds.). "Sulfur isotopes." In Encyclopedia of Geobiology (Encyclopedia of Earth Sciences Series). Springer, Dordrecht, Netherlands. https://doi.org/10.1007/978-1-4020-9212-1.

Bottrell, S.H., Newton, R.J. (2006). Reconstruction of changes in global sulfur cycling from marine sulfate isotopes. Earth-Science Reviews, 75, 59–83. https://doi.org/10.1016/j. earscirev.2005.10.004.

Bruska, S. Mamand, D., Mawlood, K. (2024). Identifying sources of groundwater and recharge zone using stable environmental isotopes in the Erbil basin-northern Iraq, Kuwait Journal of Science. 51(1), 100128, ISSN 2307-4108.

Cartwright, I., Weaver, T., Tweed, S., Ahearne, D., Cooper, M., Czapnik, K., Tranter, J. (2002). Stable isotope geochemistry of cold CO2-bearing mineral spring waters, Daylesford, Victoria, Australia: sources of gas and water and links with waning volcanism. Chemical Geologyl. 185, 71-91. http://dx.doi.org/10.1016/S0009-2541(01) 00397-7.

Chunlu, J., Lili, C., Chang, Li., Liugen, Z. (2022). A hydrochemical and multi-isotopic study of groundwater sulfate origin and contribution in the coal mining area, Ecotoxicology and Environmental Safety, Vol. 248, 114286, ISSN 0147-6513, https://doi.org/10.1016/ j.ecoenv.2022.114286.

Connor, P. N., Katherine, W.D., Robert, L.R. , Richard, T.W. (2023). Mechanisms of water-rock interaction and implications for remediating flooded mine workings elucidated from environmental tracers, stable isotopes, and rare earth elements. Applied Geochemistry, 157, 105769. https://doi.org/10.1016/j.apgeochem.2023.105769.

Dansgaard W. (1964). Stable isotopes in precipitation," Tellus, 16(4): 436–468. http://dx.doi.org/10.1111/j.2153-3490.1964.tb00181.x.

Gibbs, R. J. (1970). Mechanism controlling world water chemistry. The Sciences, New Series, 170, 3962, 1088-1090. http://www.jstor.org/stable/1730827.

Drost, W and Klotz, D. (1983). Aquifer Characteristics, In: Guidebook on Nuclear Techniques in Hydrology, IAEA, Vienna. https://doi.org/10.1177/030913338601000104.

Equeenuddin, S.M., Tripathy, S., Sahoo, P.K., Panigrahi, M.K. (2010). Hydro-geochemical characteristics of acid mine drainage and water pollution at Makum Coalfield, India. Journal of Geochemical Exploration, 105(3), 75–82. https://doi.org/10.1016/j.gexplo.2010.04.006.

Frenzel, W., Michalski, R. (2016). Sample preparation techniques for ion chromatography. Application of IC-MS and IC-ICP-MS in Environmental Research, 210–266. https://doi.org/10.1002/9781119085362.ch8.

Fryar, A.E., Barna, J.M., Benaabidate, L., Howell, B.A., Mehta, S., Mukherjee, A. (2021). Using oxygen-18 and deuterium to delineate groundwater recharge at different spatial and temporal scales. Hydrological Aspects of Climate Change, 303–312. DOI:10.1007/978-981-16-0394-5_16.

Fynn, O.F., Yidana, S.M., Chegbeleh, I.P., Yiran, G.B. (2016). Evaluating groundwater recharge processes using stable isotope signatures–The Nabogo catchment of the White Volta, Ghana. Arabian Journal of Geosciences, 9, 1-15. DOI 10.1007/s12517-015-2299-0.

Gat, J.R. (1996). Oxygen and hydrogen isotopes in the hydrologic cycle. Annual Review of Earth and Planetary Sciences, 24 (1), 225–262. 10.1146/annurev.earth.24.1.225.

Guan, Z., Jia, Z., Zhao, Z., You, Q. (2019). Identification of inrush water recharge sources using hydrochemistry and stable isotopes: A case study of Mindong No. 1 coalmine in northeast Inner Mongolia, China. Journal of Earth System Science, 128, 7. DOI:10.1007/s12040-019-1232-4.

Gammons, C.H., Nimick, D.A., Parker, S.R. (2015). Diel cycling of trace elements in streams draining mineralized areas – a review. Applied Geochemistry, 57, 35–44. https:// doi.org/10.1016/j.apgeochem.2014.05.008.

Halevy, E. (1967). Borehole dilution techniques: A critical review, in: Isotopes in Hydrology, IAEA Vienna. 531-64, NSA-22-019070. https://www.osti.gov/biblio/4556505.

IAEA, Introduction to Water Sampling and Analysis for Isotope Hydrology, Non-serial Publications (2007), IAEA, Vienna.

Ibrahim, S.M. (2009). Stratigraphy of Pakistan, Geological Survey of Pakistan, 25-39.

Klotz, D. (1978). a - Werte Ausgebauter Bohrungen, *"Values for completed boreholes"*, Gesellschaftfur Strahlen-und Umweltforschung mbH Institut fur Radiohydrometrie, GSF-Bericht R- 176.

Khan, A. J., Akhter, G., Gabriel, H. F., Shahid, M. (2020). Anthropogenic effects of coal mining on ecological resources of the central indus basin, Pakistan. Int. J. of Env. Res. and Pub. Health, 17(4). https://doi.org/10.3390/ijerph17041255.

Kumar, P., Singh, A.K. (2022). Hydrogeochemistry and quality assessment of surface and sub-surface water resources in Raniganj coalfield area, Damodar Valley, India. International Journal of Environmental Analytical Chemistry,102 (19), 8346–8369. https://doi.org/10.1080/ 03067319.2020.1849653.

Li, P., Wu, J., Tian, R., He, S., He, X., Xue, C., Zhang, K. (2018). Geochemistry, Hydraulic Connectivity and Quality Appraisal of Multilayered Groundwater in the Hongdunzi Coal Mine, Northwest China. Mine Water and the Environment, 37(2), 222–237. https://doi.org/10.1007/ s10230-017-0507-8.

Liu, Y., Wei, L., Wu, Q., Luo, D., Xiao, T., Wu, Q., Huang, X., Liu, J., Wang, J., & Zhang, P. (2022). Impact of acid mine drainage on groundwater hydrogeochemistry at a pyrite mine (South China): a study using stable isotopes and multivariate statistical analyses. Environmental Geochemistry and Health, 45(3), 771–785. https://doi.org/10.1007/s10653-022-01242-8.

Liu, J., Li, S., Zhong, J., Zhu, X., Guo, Q., Lang, Y. and Han, X. (2017). Sulfate sources constrained by sulfur and oxygen isotopic compositions in the upper reaches of the Xijiang River, China. Acta Geochimica, 36, 611-618. DOI:10.1007/s11631-017-0175-1.

Malkani, M. S., & Malik, Z. M. (2018). Revised Stratigraphy and Mineral Resources of Sulaiman Basin, Pakistan Geological Survey of Pakistan, Information Release (GSP IR), 1003, 1-63. https://www.researchgate.net/publication/315834399.

Nordstrom, D.K. (2011). Hydro-geochemical processes governing the origin, transport and fate of major and trace elements from mine wastes and mineralized rock to surface waters. Applied Geochemistry, 26 (11), 1777–1791. https://doi.org/10.1016/j.apgeochem.2011.06.002.

Odri, A., Becker, M., Broadhurst, J., Harrison, S. T. L., Edraki, M. (2020). Stable Isotope Imprints during Pyrite Leaching: Implications for Acid Rock Drainage Characterization. Minerals, 10(11), 982. https://doi.org/10.3390/min10110982

Perez, L. R., Delgado, J., Nieto, J.M., Arquez-Garcia, B. (2010). Rare earth element geochemistry of sulphide weathering in the Sao Domingos mine area (Iberian Pyrite Belt): A proxy for fluid–rock interaction and ancient mining pollution. Chemical Geology, 276 (1–2), 29–40. https://doi.org /10.1016/j.chemgeo.2010.05.018.

Piper, A. M. (1953). A graphic procedure in the geo-chemical interpretation of water analyses." USGS Groundwater Note no. 12, 25(6). https://doi.org/10.1029/TR025i006p00914.

Prathap, A., Chakraborty, S. (2019). Hydro chemical characterization and suitability analysis of groundwater for domestic and irrigation uses in open cast coal mining areas of Charhi and Kuju, Jharkhand, India. Groundwater for Sustainable Developement, 9, 100244.

Qu, S., Duan, L., Mao, H., Wang, C., Liang, X., Luo, A., et al. (2023). Hydrochemical and isotopic fingerprints of groundwater origin and evolution in the Urangulan River basin, China's Loess Plateau. Science of The Total Environment, 866, 161377 https://doi.org/10.1016/j.scitotenv.2022.161377.

Roy, A., Keesari, T., Mohokar, H., Pant, D., Sinha, U.K., Mendhekar, G.N. (2020). Geochemical evolution of groundwater in hard-rock aquifers of South India using statistical and modelling techniques. Hydrological Sciences Journal, 65 (6), 951–968. https://doi. org/10.1080/02626667.2019.1708914.

Rozanski, K., Araguás, L. A., Gonfiantini R. (2019). Isotopic Patterns in Modern Global Precipitation, Geophysical Monograph Series. https://doi.org/10.1029/GM078p0001.

Rozanski, K., Araguás, L. A., Gonfiantini R. (1992). Relation Between Long-Term Trends of Oxygen-18 Isotope Composition of Precipitation and Climate. Science, 258, 5084, 981-985. DOI: 10.1126/science.258.5084.981.

Rye, R.O., Back, W., Hanshaw, B.B., Rightmire, C.T., Pearson, F.J. (1981). The origin and isotopic composition of dissolved sulfide in groundwater from carbonate aquifers in Florida and Texas. Geochimica et Cosmochimica Acta, 45 (10), 1941–1950. https://doi.org/10.1016/0016-7037(81)90024-7.

Ruta, K., Sascha, S., Gareth, J., Stuart, M.V. G. (2017). The influence of oxygen isotope exchange between CO_2 and H_2O in natural CO_2-rich spring waters: Implications for geothermometry, Applied Geochemistry, 84, 173-186, ISSN 0883-2927.

Sahoo, S., Khaoash, S. (2020). Impact assessment of coal mining on groundwater chemistry and its quality from Brajrajnagar coal mining area using indexing models. Journal of Geochemical Exploration, 215, 106559. DOI:10.1016/j.gexplo.2020.106559

Seal II, R.R. (2006). Sulfur isotope geochemistry of sulfide minerals. Reviews in Mineralogy and Geochemistry. 61 (1), 633–677. DOI:10.2138/rmg.2006.61.12

Schoeller, H. (1967). Qualitative Evaluation of Ground Water Resources. In: Schoeller, H., Ed., Methods and Techniques of Groundwater Investigation and Development, Water Resource Series No. 33, UNESCO, Paris, 44-52.

Shah, H., Khan, M.A., Akmal, N. (2005). Livelihood assets and livelihood strategies of small farmers in Salt Range: a case study of Pind Dadan Khan District Jhelum, Pakistan Journal of Agricultural Research, 42, 1-2.

Spangenberg, J.E., Dold, B., Vogt, M.L., Pfeifer, H.R. (2007). Stable hydrogen and oxygen isotope composition of waters from mine tailings in different climatic environments. Environmental Science and Technology, 41 (6), 1870–1876. DOI:10.1021/es061654w.

Sreedevi, P.D., Sreekanth, P.D. Reddy, D.V. (2021). Deuterium Excess of Groundwater as a Proxy for Recharge in an Evaporative Environment of a Granitic Aquifer, South India. Journal of the Geological Society India, 97, 649–655. https://doi.org/10.1007/s12594-021-1740-0.

Syed, M. A., Syed, M. T., Muhammad, S., Muhammad, Z., Abu, B., Muhammad, W., 2015. Water Characterization of Coal Mining Areas of Chakwal, Punjab, Pakistan. Pakistan Journal of Scientific and Industrial Research Series A: Physical Sciences, 58 (1), 41-45.

Tianming, H., Zhonghe, P. (2012). The role of deuterium excess in determining the water salinisation mechanism: A case study of the arid Tarim River Basin, NW China. Applied Geochemistry, 27, 2382–2388. DOI:10.1016/j.apgeochem.2012.08.015.

Thomas, R., Martin, D., Jessica, A. Stammeier, A. L., Diego B. G., Sylke H. (2020). Geochemistry of coal mine drainage, groundwater, and brines from the Ibbenbüren mine, Germany: A coupled elemental-isotopic approach, Applied Geochemistry, 121, 104693, ISSN 0883-2927.

Wellen, C., Shatilla, N. J., Carey, S. K. (2018). The influence of mining on hydrology and solute transport in the Elk Valley, British Columbia, Canada. Environmental Research Letters, 13, 7, DOI:10.1088/1748-9326/aaca9d.

Wilcox, L. V. (1955). Classification and use of irrigation water, US Department of agriculture, Washington DC, 19. https://ia803201.us.archive.org/10/items/classificationus969wilc/ classificationus 969 wilc.pdf.

Yang, K., Han, G. (2020). Controls over hydrogen and oxygen isotopes of surface water and groundwater in the Mun River catchment, northeast Thailand: implications for the water cycle. Hydrogeology Journal. 28 (3). https://doi.org/10.1007/s10040-019-02106-9.

Wang Z., Xu, Y., Zhang, Z., Zhang,Y. (2021). Review: Acid Mine Drainage (AMD) in Abandoned Coal Mines of Shanxi, China. Water, 13,1, 8. https://doi.org/10.3390/w13010008.

Zongjun, G., Jiutan, L., Jianguo, F., Min, W., Guangwei, W. (2019). Hydrogeochemical characteristics and the suitability of groundwater in the Alluvial-Diluvial plain of Southwest Shandong Province, China, Water, 11, 1577. DOI:10.3390/w11081577.